Supplement of

Enhanced sulfate formation in mixed biomass burning and sea-salt interactions mediated by photosensitization: effects of chloride, nitrogen-containing compounds, and atmospheric aging

Rongzhi Tang et al.

Correspondence to: Chak K. Chan (chak.chan@kaust.edu.sa)

S1. Chemical analysis

The sulfate, nitrate and chloride anions in the BB extracts were analyzed by a Dionex ion chromatography (IC, Dionex ICS-1100, Sunnyvale, CA) with a Dionex AS-DV autosampler (Sunnyvale, CA). The key analytical system includes a suppressed conductivity detector (Sunnyvale, CA), a self-regenerating anion suppressor (ASRS 300) and an AS 11 analytical column.

The particulate organic matter collected on BB filters were analyzed by a comprehensive two-dimensional gas chromatography-mass spectrometry (GC×GC-MS, GC-MS TQ 8050, SHIMADZU, Japan) coupled with a thermal desorption module (TDS 3, C506, Gerstel). The first column of GC×GC was non-polar SH-Rxi-1ms (30 m × 0.25 mm × 0.25 μm) and second column was mid-polar BPX50 (2.5 m × 0.1 mm × 0.1 μm). The modulation period was 6 s. The desorption temperature of TDS was 280 ℃. More details can be found in previous research (Song et al., 2022b; Song et al., 2022a). Water-soluble organics of the BB extracts were analyzed by an ultra-high performance liquid chromatography (Thermo Scientific Dionex UltiMate 3000 UHPLC, USA) coupled with high-resolution Orbitrap Fusion Lumos Tribrid mass spectrometry (UHPLC-Orbitrap-HR-MS, Thermo Fisher Scientific, USA). Chromatographic separation was conducted using a reversed-phase column (Acquity HSS T3 column, 100×2.1 mm, 1.8 μm particle size, Waters Corp., Ireland) at 40°C, and the autosampler was cooled at 4 °C. Mobile phases included eluent A (water with 0.1% formic acid) and eluent B (acetonitrile with 0.1% formic acid). The gradient elution program consisted of a 10% B start for 1 min, increasing to 90% B over 25 min, holding for 4 min, decreasing to 10% B in 1 min, and a 5 min re-equilibration. The flow rate was 0.2 mL/min, injection volume was 10 μL. NTA software (Compound Discoverer CD, version 3.2, Thermo Fisher Scientific) was employed to identify the chromatographic peak features. Compound identification was based on the combination of features eluting at the same retention time and exhibiting m/z values corresponding to precise mass differences, including isotopes, adducts, clusters, or fragments. In all the experiments, threshold intensities of 1E5 (low) and 1E10 (high) were applied to the two-dimensional coordinate system (RT: 1-20 min, m/z: 50-500). The CD software automatically excluded ions with peak abundances below or above the threshold.

The identified molecular formula, mainly $C_cH_hO_oN_nS_s$, were classified into different categories, namely, CHO, CHON, CHONS, CHOS and others. For example, CHON represents compounds composed solely of carbon, hydrogen, oxygen and nitrogen elements. The "others" category includes compounds not falling into CHO, CHON, CHONS, or CHOS, as well as signals without calculated elemental formulas. Molecular formulas were also categorized according to their elemental ratios, e.g. H/C, O/C, N/C, double bond equivalents (DBE), modified aromaticity index (AI_{mod}) and maximum carbonyl ratio (MCR). The DBE, AI_{mod} and MCR (Zhang et al., 2021) were calculated as:

$$DBE=1+c-0.5h+0.5n \tag{S1}$$

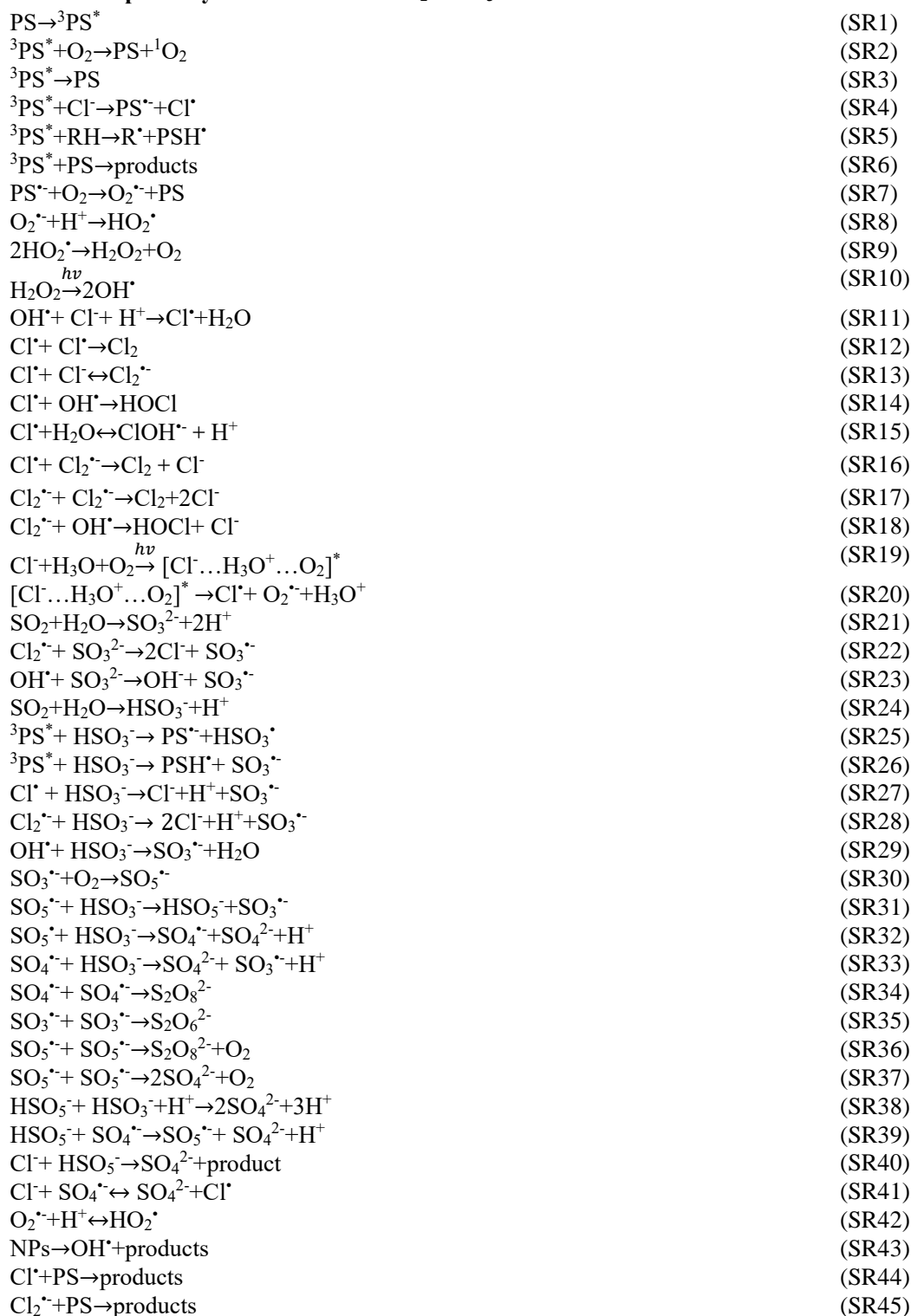$$AI_{mod}=\frac{DBE_{AI}}{C_{AI}} = \frac{1+c-0.5o-s-0.5(n+h)}{c-0.5o-n-s} \tag{S2}$$

$$MCR = \frac{DBE}{o} \tag{S3}$$

In which c, h, o and n corresponds to the number of C, H, O and N atoms, respectively in the assigned molecular formula. Formula were categorized into six groups, i.e., condensed aromatics ($AI_{mod} \geq 0.67$), polyphenolics ($0.50 < AI_{mod} < 0.67$), highly unsaturated and phenolic formula ($AI_{mod} \leq 0.5$, H/C < 1.5), aliphatics (H/C≥1.5, O/C≤0.9, N=0), peptide-like formula (H/C≥1.5,

O/C≤0.9, N=0) and sugar-like formula (H/C≥1.5, O/C > 0.9) (Zherebker et al., 2022; Koch and Dittmar, 2006). For MCR, here we only applied it in CcHhOo compounds. The Equation S3 fits for compounds with larger or equal atom O compared to DBE. If the atom O in CcHhOo is smaller than DBE, then MCR is considered to be 1, i.e., all the O atoms contribute to DBE.

S2. Possible pathways involved in the SO_2/HSO_3^- oxidation

$PS \rightarrow {}^3PS^*$ (SR1)

${}^3PS^* + O_2 \rightarrow PS + {}^1O_2$ (SR2)

${}^3PS^* \rightarrow PS$ (SR3)

${}^3PS^* + Cl^- \rightarrow PS^{\bullet-} + Cl^{\bullet}$ (SR4)

${}^3PS^* + RH \rightarrow R^{\bullet} + PSH^{\bullet}$ (SR5)

${}^3PS^* + PS \rightarrow products$ (SR6)

$PS^{\bullet-} + O_2 \rightarrow O_2^{\bullet-} + PS$ (SR7)

$O_2^{\bullet-} + H^+ \rightarrow HO_2^{\bullet}$ (SR8)

$2HO_2^{\bullet} \rightarrow H_2O_2 + O_2$ (SR9)

$H_2O_2 \xrightarrow{h\nu} 2OH^{\bullet}$ (SR10)

$OH^{\bullet} + Cl^- + H^+ \rightarrow Cl^{\bullet} + H_2O$ (SR11)

$Cl^{\bullet} + Cl^{\bullet} \rightarrow Cl_2$ (SR12)

$Cl^{\bullet} + Cl^- \leftrightarrow Cl_2^{\bullet-}$ (SR13)

$Cl^{\bullet} + OH^{\bullet} \rightarrow HOCl$ (SR14)

$Cl^{\bullet} + H_2O \leftrightarrow ClOH^{\bullet-} + H^+$ (SR15)

$Cl^{\bullet} + Cl_2^{\bullet-} \rightarrow Cl_2 + Cl^-$ (SR16)

$Cl_2^{\bullet-} + Cl_2^{\bullet-} \rightarrow Cl_2 + 2Cl^-$ (SR17)

$Cl_2^{\bullet-} + OH^{\bullet} \rightarrow HOCl + Cl^-$ (SR18)

$Cl^- + H_3O + O_2 \xrightarrow{h\nu} [Cl^- \ldots H_3O^+ \ldots O_2]^*$ (SR19)

$[Cl^- \ldots H_3O^+ \ldots O_2]^* \rightarrow Cl^{\bullet} + O_2^{\bullet-} + H_3O^+$ (SR20)

$SO_2 + H_2O \rightarrow SO_3^{2-} + 2H^+$ (SR21)

$Cl_2^{\bullet-} + SO_3^{2-} \rightarrow 2Cl^- + SO_3^{\bullet-}$ (SR22)

$OH^{\bullet} + SO_3^{2-} \rightarrow OH^- + SO_3^{\bullet-}$ (SR23)

$SO_2 + H_2O \rightarrow HSO_3^- + H^+$ (SR24)

${}^3PS^* + HSO_3^- \rightarrow PS^{\bullet-} + HSO_3^{\bullet}$ (SR25)

${}^3PS^* + HSO_3^- \rightarrow PSH^{\bullet} + SO_3^{\bullet-}$ (SR26)

$Cl^{\bullet} + HSO_3^- \rightarrow Cl^- + H^+ + SO_3^{\bullet-}$ (SR27)

$Cl_2^{\bullet-} + HSO_3^- \rightarrow 2Cl^- + H^+ + SO_3^{\bullet-}$ (SR28)

$OH^{\bullet} + HSO_3^- \rightarrow SO_3^{\bullet-} + H_2O$ (SR29)

$SO_3^{\bullet-} + O_2 \rightarrow SO_5^{\bullet-}$ (SR30)

$SO_5^{\bullet-} + HSO_3^- \rightarrow HSO_5^- + SO_3^{\bullet-}$ (SR31)

$SO_5^{\bullet-} + HSO_3^- \rightarrow SO_4^{\bullet-} + SO_4^{2-} + H^+$ (SR32)

$SO_4^{\bullet-} + HSO_3^- \rightarrow SO_4^{2-} + SO_3^{\bullet-} + H^+$ (SR33)

$SO_4^{\bullet-} + SO_4^{\bullet-} \rightarrow S_2O_8^{2-}$ (SR34)

$SO_3^{\bullet-} + SO_3^{\bullet-} \rightarrow S_2O_6^{2-}$ (SR35)

$SO_5^{\bullet-} + SO_5^{\bullet-} \rightarrow S_2O_8^{2-} + O_2$ (SR36)

$SO_5^{\bullet-} + SO_5^{\bullet-} \rightarrow 2SO_4^{2-} + O_2$ (SR37)

$HSO_5^- + HSO_3^- + H^+ \rightarrow 2SO_4^{2-} + 3H^+$ (SR38)

$HSO_5^- + SO_4^{\bullet-} \rightarrow SO_5^{\bullet-} + SO_4^{2-} + H^+$ (SR39)

$Cl^- + HSO_5^- \rightarrow SO_4^{2-} + product$ (SR40)

$Cl^- + SO_4^{\bullet-} \leftrightarrow SO_4^{2-} + Cl^{\bullet}$ (SR41)

$O_2^{\bullet-} + H^+ \leftrightarrow HO_2^{\bullet}$ (SR42)

$NPs \rightarrow OH^{\bullet} + products$ (SR43)

$Cl^{\bullet} + PS \rightarrow products$ (SR44)
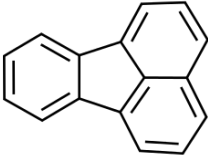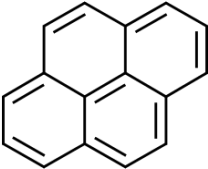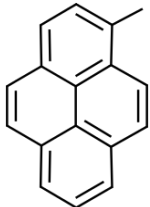
$Cl_2^{\bullet-} + PS \rightarrow products$ (SR45)

Table S1. Chemical compositions in extracted BB and IS extracts.

Category	TOC (mg L^{-1})	Cr (μg L^{-1})	Cu (μg L^{-1})	Fe (μg L^{-1})	Mn (μg L^{-1})	Ni (μg L^{-1})	Ti (μg L^{-1})	Zn (μg L^{-1})	Cl$^-$ (mg L^{-1})	SO$_4$$^{2-}$ (mg L^{-1})	NO$_3$$^-$ (mg L^{-1})	$\sum anions$[a] (mg L^{-1})	$\dfrac{\sum anions}{TOC}$
RS$_F$	69.9	1.8	0	31.7	5.8	0	73.0	74.5	44.1	6.0	3.2	53.3	0.8
WS$_F$	64.5	2.3	4.6	96.9	2.9	1.2	94.2	30.3	41.1	5.2	3.1	49.4	0.8
CS$_F$	45.6	0.9	0	31.9	3.5	0	76.9	29.1	9.5	4.5	3.2	17.2	0.4
IS$_F$	571.1	1.7	23.2	12.5	7.6	0.7	9.1	77.3	8.1	3.7	5.6	17.5	0.03
RS$_A$	61.4	2.6	39.5	87.5	5.2	0.5	76.3	59.5	35.5	5.2	3.1	43.7	0.7
WS$_A$	52.7	4.8	31.6	176.7	3.3	1.6	43.7	26.0	39.9	4.9	3.1	47.9	0.9
CS$_A$	34.0	2.7	21.8	111.8	3.4	0.5	21.3	26.0	16.9	4.0	3.1	24.0	0.7
IS$_A$	584.8	4.2	33.7	87.9	10.1	0.8	17.0	100.1	8.4	4.3	5.6	18.4	0.03

$$\sum anions = [Cl^-] + [SO_4^{2-}] + [NO_3^-]$$

Table S2. Possible photosensitizers, formulas and structures in BB extracts detected by state-of-art mass spectrometer.

Category	Possible photosensitizers	Formula	Calc. MW	Possible structure	Detected by
PAHs	Fluoranthene	C16H10	202.256		GC×GC-MS
	Pyrene	C16H10	202.256		GC×GC-MS
	1-methylpyrene	C17H12	216.277		GC×GC-MS
	4-methylphenanthrene	C15H12	192.256		GC×GC-MS

3,6-dimethylphenanthrene	C16H14	206.282		GC×GC-MS
2-phenylnaphthalene	C16H12	204.266		GC×GC-MS
Retene	C18H18	234.335		GC×GC-MS
4,5-dihydropyrene	C16H12	204.266		GC×GC-MS
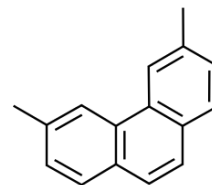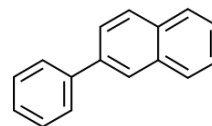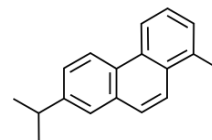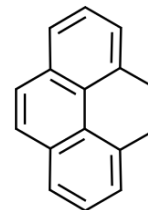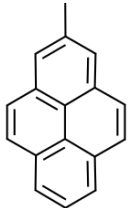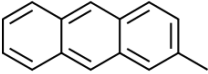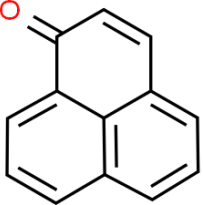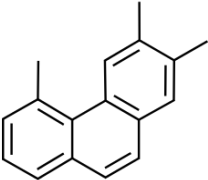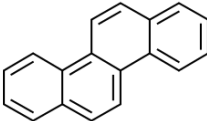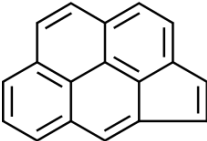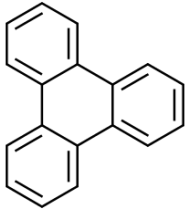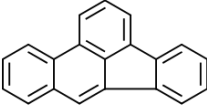
2-methylpyrene	C17H12	216.277		GC×GC-MS
2-methylanthracene	C15H12	192.256		GC×GC-MS
1H-Phenalen-1-one	C13H8O	180.202		GC×GC-MS
2,3,5-trimethylphenanthrene	C17H16	220.309		GC×GC-MS
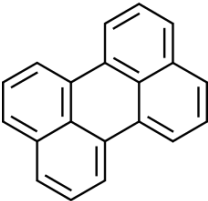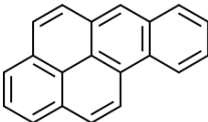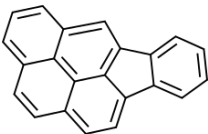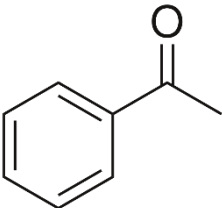
Chrysene	C18H12	228.288		GC×GC-MS
Cyclopenta[cd]pyrene	C18H10	226.272		GC×GC-MS
Triphenylene	C18H12	228.288		GC×GC-MS
Benzo[b]fluoranthene	C20H12	252.309		GC×GC-MS
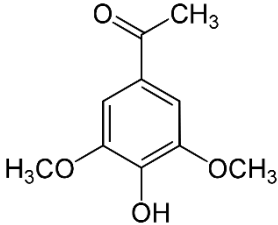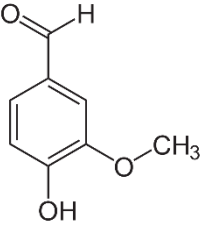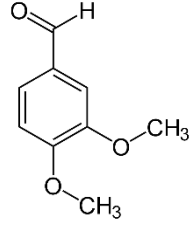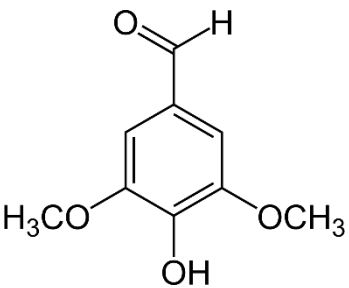
Perylene	C20H12	252.309		GC×GC-MS
Benzo[a]pyrene	C20H12	252.309		GC×GC-MS
Indeno[1,2,3-cd]pyrene	C22H12	276.331		GC×GC-MS
Acetophenone	C8H8O	120.151		GC×GC-MS UHPLC-Orbitrap-MS (ESI+)

Acetosyringone	C10H12O4	196.202		GC×GC-MS Orbitrap-MS (ESI-)
Vanillin	C8H8O3	152.149		GC×GC-MS Orbitrap-MS (ESI-)
3,4-dimethoxybenzaldehyde	C9H10O3	166.176		GC×GC-MS Orbitrap-MS (ESI-)
Syringaldehyde	C9H10O4	182.17		GC×GC-MS Orbitrap-MS (ESI-)

| Furfural | C5H4O2 | 96.08 | | Orbitrap-MS (ESI-) |
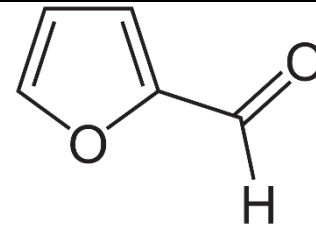
Table S3. Possible acids and formula in BB extracts by ESI- mode. Note that the acids listed appeared at least in six BB extracts.

Possible acids	Formula	Calc. MW
Citraconic acid	C5H6O4	130.0265
Homovanillic acid	C9H10O4	182.0579
Vanillic acid	C8H8O4	168.0423
Succinic acid	C4H6O4	118.0265
3-Methylsalicylic acid	C8H8O3	152.0473
2-Methylbenzoic acid	C8H8O2	136.0524
3,5-Dihydroxybenzoic acid	C7H6O4	154.0266
Salicylic acid	C7H6O3	138.0317
Azelaic acid	C9H16O4	188.1049
Glutaric acid	C5H8O4	132.0422
Sorbic acid	C6H8O2	112.0523
Methylsuccinic acid	C5H8O4	132.0422
3-Allyl-2-hydroxybenzoic acid	C10H10O3	178.063
trans-Cinnamic acid	C9H8O2	148.0524
Ferulic acid	C10H10O4	194.0579
Homogentisic acid	C8H8O4	168.0423
2-Hydroxycinnamic acid	C9H8O3	164.0474
2,3-Dihydro-1-benzofuran-2-carboxylic acid	C9H8O3	164.0473
DL-Mandelic acid	C8H8O3	152.0473

6-Methoxysalicylic acid	C8H8O4	168.0423
Isophthalic acid	C8H6O4	166.0266
Phenylglyoxylic acid	C8H6O3	150.0317
4-Hydroxyphenylpyruvic acid	C9H8O4	180.0423
Syringic acid	C9H10O5	198.0529
2-Methylglutaric acid	C6H10O4	146.0579
BMK glycidic acid	C10H10O3	178.063
Caffeic acid	C9H8O4	180.0423
2-Anisic acid	C8H8O3	152.0473
6-Hydroxypicolinic acid	C6 H5NO3	139.0269
4-Hydroxymandelic acid	C8H8O4	168.0423
Homovanillic acid	C9H10O4	182.0579
6-Hydroxy-2-naphthoic acid	C11H8O3	188.0474
3-Methoxyphenylacetic acid	C9H10O3	166.063
Sinapinic acid	C11H12O5	224.0685

Table S4. Shapiro-Wilk normality test results for the analysis of correlation coefficients.

Parameter	Statistic	p-value	Decision at level (5%)
k_{SO4}	0.90341	0.17551	Can't reject normality
Chloride	0.66506	3.96E-04	Reject normality
Fe	0.83678	0.02531	Reject normality
Mn	0.79415	0.00804	Reject normality
Sulfate	0.70692	9.83E-04	Reject normality
Nitrate	0.87657	0.07923	Can't reject normality
CHO-	0.80111	0.00964	Reject normality
CHON-	0.78144	0.00581	Reject normality
Others-	0.78595	0.00651	Reject normality
CHO+	0.68063	5.52E-04	Reject normality
CHON+	0.7749	0.00492	Reject normality
CHN+	0.86772	0.06114	Can't reject normality
Others+	0.88449	0.10007	Can't reject normality

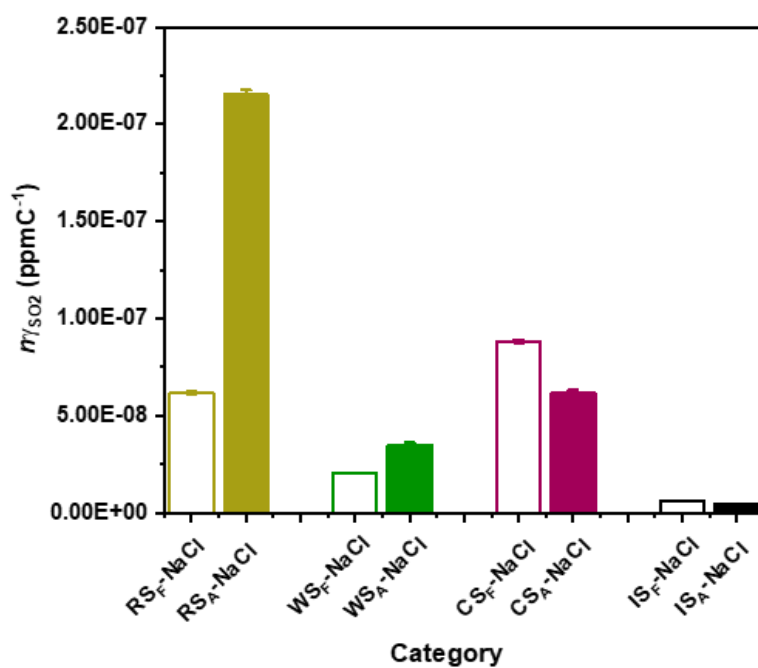**Figure S1.** Image of the iron stove used in this study.

Figure S2. Differences of normalized SO$_2$ uptake coefficients $n\gamma_{SO2}$ between fresh and aged BB-NaCl droplets.
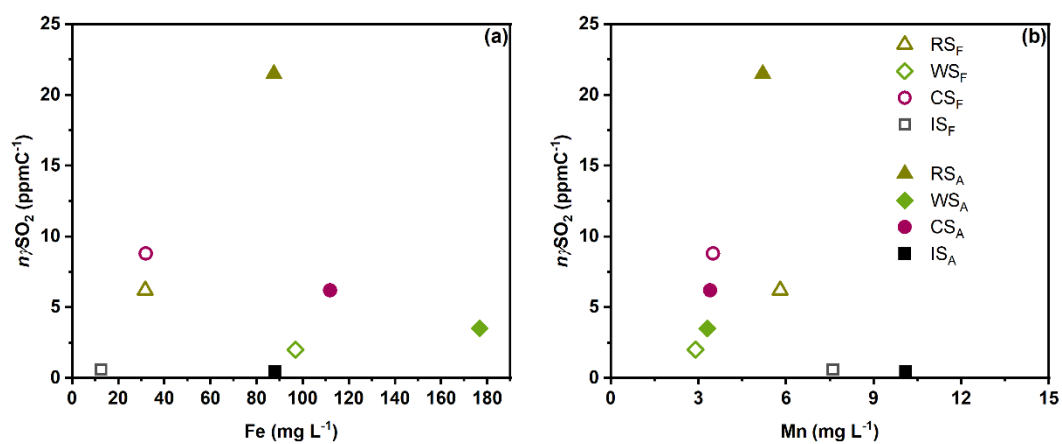
Figure S3. Correlation of (a) Fe and (b) Mn concentration with normalized SO_2 uptake coefficient $(n\gamma_{SO_2})$
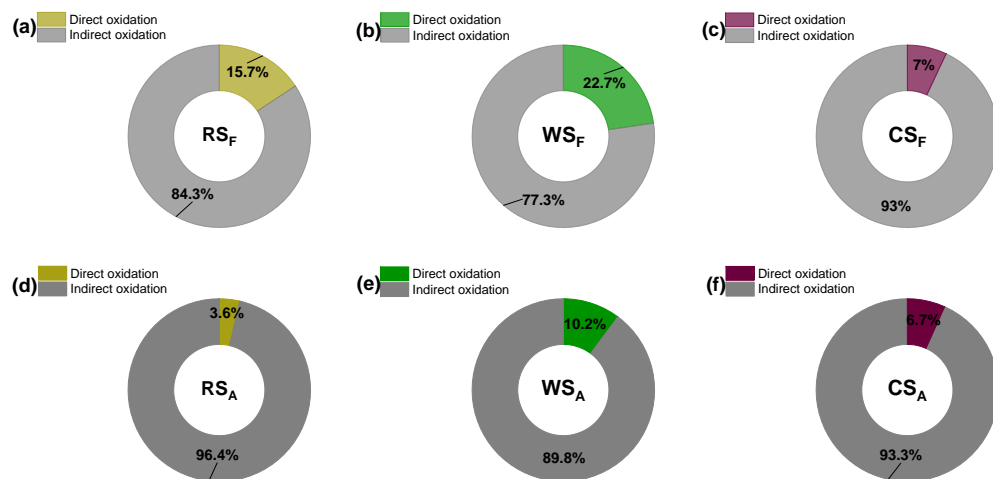
Figure S4. Contributions of direct and indirect PS* oxidation to sulfate in droplet experiments
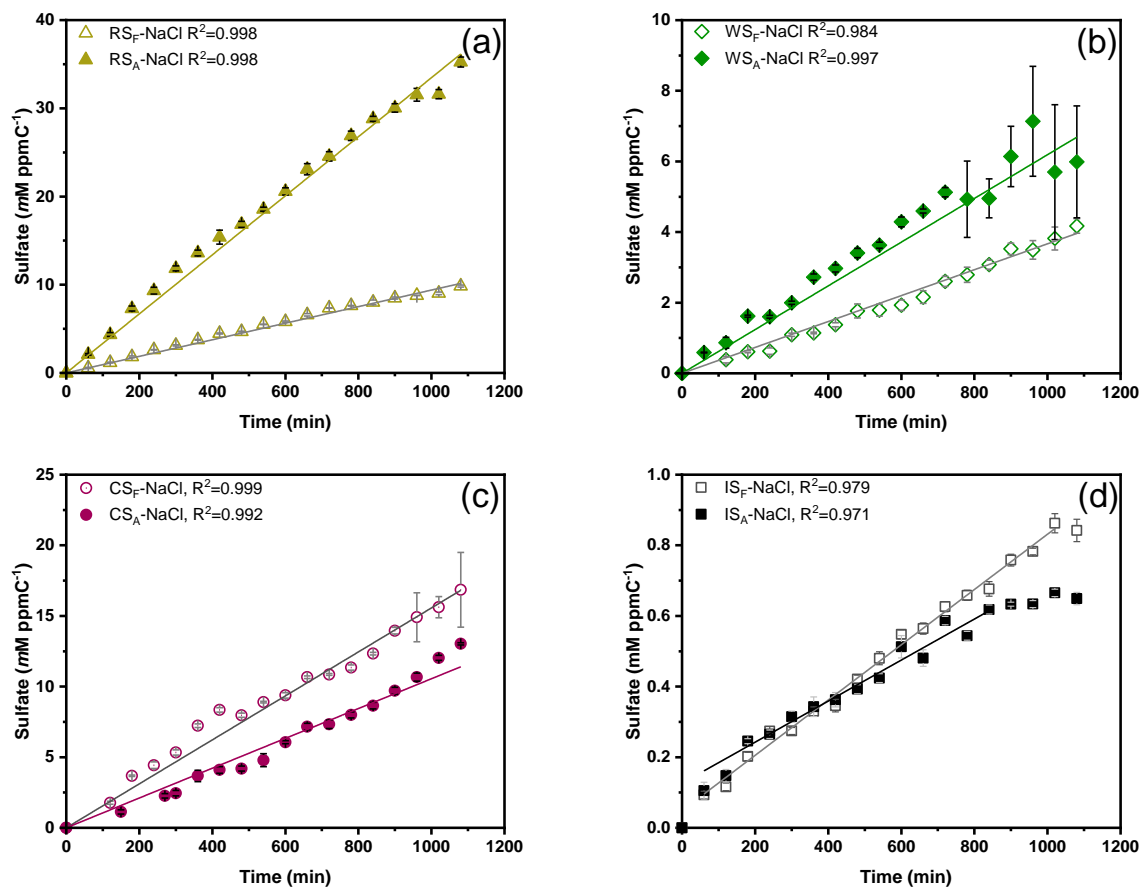
Figure S5. Sulfate production under different droplet compositions (fresh or aged BB-NaCl) as a function of time: (a) $RS_{F/A}$-NaCl droplets; (b) $WS_{F/A}$-NaCl droplets; (c) $CS_{F/A}$-NaCl droplets; (d) $IS_{F/A}$ droplets.
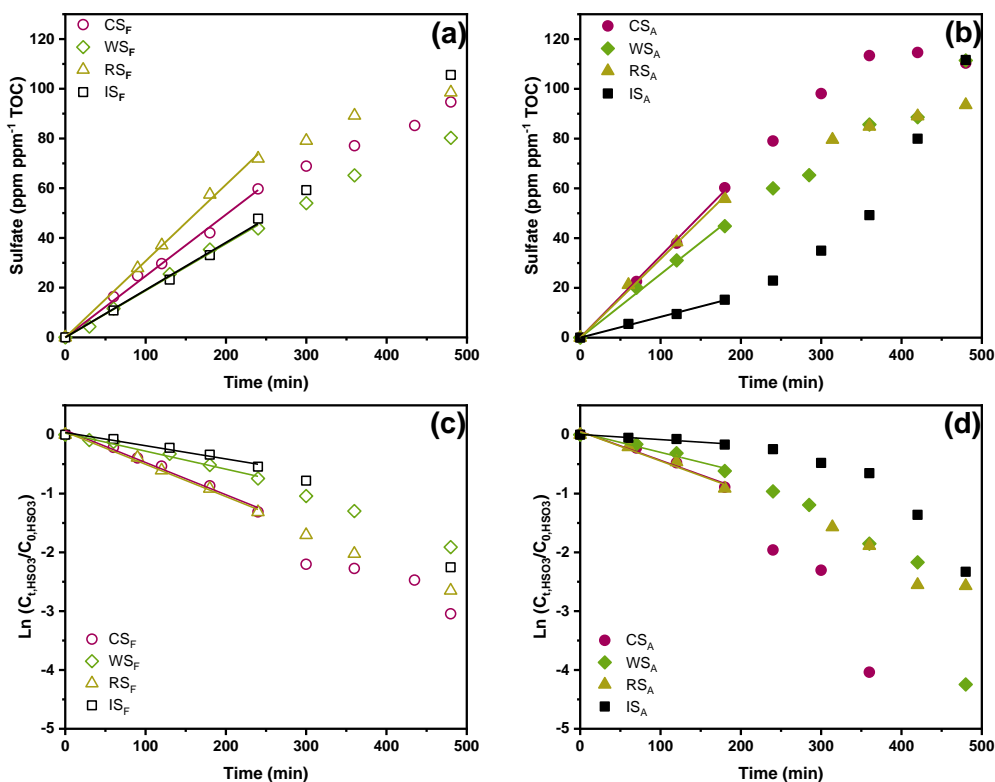
Figure S6. Concentration changes of (a)(b) sulfate and (c)(d) bisulfite using different BB extracts as a function of time, in which (a)(c) represent the results of fresh BB extracts, and (b)(d) represent the results of aged BB extracts.
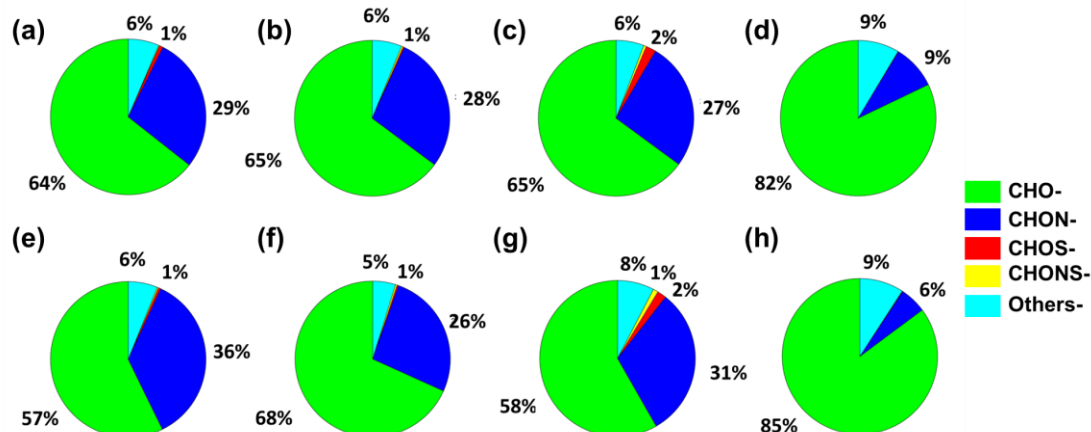
Figure S7. The intensity contribution (%) of each compound category to the total detected compound intensity: (a) RS_F; (b) WS_F; (c) CS_F; (d) IS_F; (e) RS_A; (f) WS_A; (g) CS_A; (h) IS_A by ESI-mode.
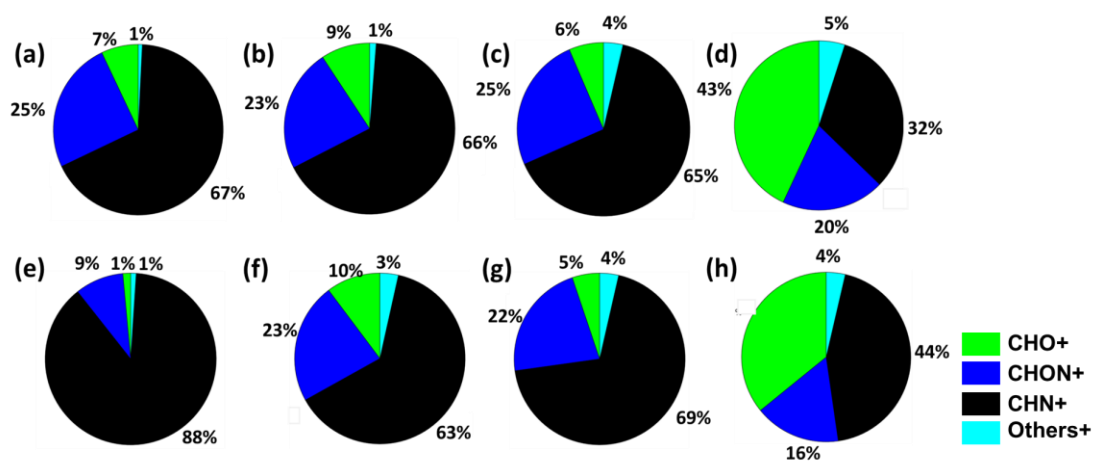
Figure S8. The intensity contribution (%) of each compound category to the total detected compound intensity: (a) RS_F; (b) WS_F; (c) CS_F; (d) IS_F; (e) RS_A; (f) WS_A; (g) CS_A; (h) IS_A by ESI+ mode.
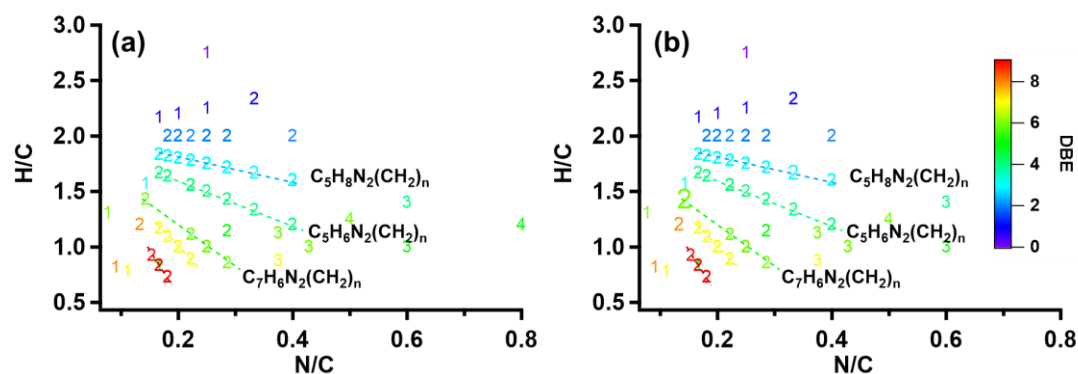
Figure S9. Van Krevelen plots of N-bases in (a) RS_F and (b) RS_A. The color bar represents the double bond equivalent, and the text marker denotes the nitrogen number in each assigned formula. Points that share the same number of nitrogen atoms and are positioned in a linear arrangement belong to identical homologous series based on CH_2. These series are characterized by a core molecule combined with $(CH_2)_n$ units, where n is equal to or greater than zero.

|	kSO4	Chloride	Fe	Mn	Sulfate	Nitrate	CHO-	CHON-	Others-	CHO+	CHON+	CHN+	Others+
kSO4	kSO4			*			*	*		*		*	
Chloride	0.16	Chloride							*				*
Fe	0.58	0.27	Fe			*							
Mn	0.72	0.43	0.45	Mn			*	*		*		*	
Sulfate	0.21	0.21	0.45	0.46	Sulfate								
Nitrate	0.65	0.085	0.83	0.56	0.69	Nitrate							
CHO-	-0.75	-0.52	-0.37	-0.94	-0.22	-0.44	CHO-	*		*		*	
CHON-	0.74	0.53	0.39	0.93	0.19	0.42	-1.00	CHON-		*		*	
Others-	-0.19	-0.72	-0.38	-0.099	-0.099	-0.099	0.25	-0.27	Others-				
CHO+	-0.77	-0.38	-0.41	-0.91	-0.32	-0.60	0.94	-0.92	0.44	CHO+		*	
CHON+	-0.52	0.13	-0.19	-0.27	0.53	-0.084	0.36	-0.37	-0.11	0.35	CHON+		
CHN+	0.72	0.54	0.40	0.94	0.20	0.41	-0.99	0.99	-0.27	-0.93	-0.38	CHN+	
Others+	0.11	-0.79		-0.36	-0.13	0.19	0.48	-0.50	0.66	0.30	-0.33	-0.51	Others+

* p<=0.01

Figure S10. Heatmap of Spearman correlations between sulfate formation rate (kSO4) and other factors, including chloride, Fe, Mn, sulfate, nitrate, and different chemical species detected by ESI (-) and ESI (+) mode. Note that the calculations were based on the sulfate formation rate and the original concentrations of the influencing factors in the bulk solution. The symbol * indicates significance, i.e., $p \leqslant 0.01$. Red color means positive correlation ($r > 0$), and blue color means negative correlation ($r < 0$). The darker the color, the higher the r value.
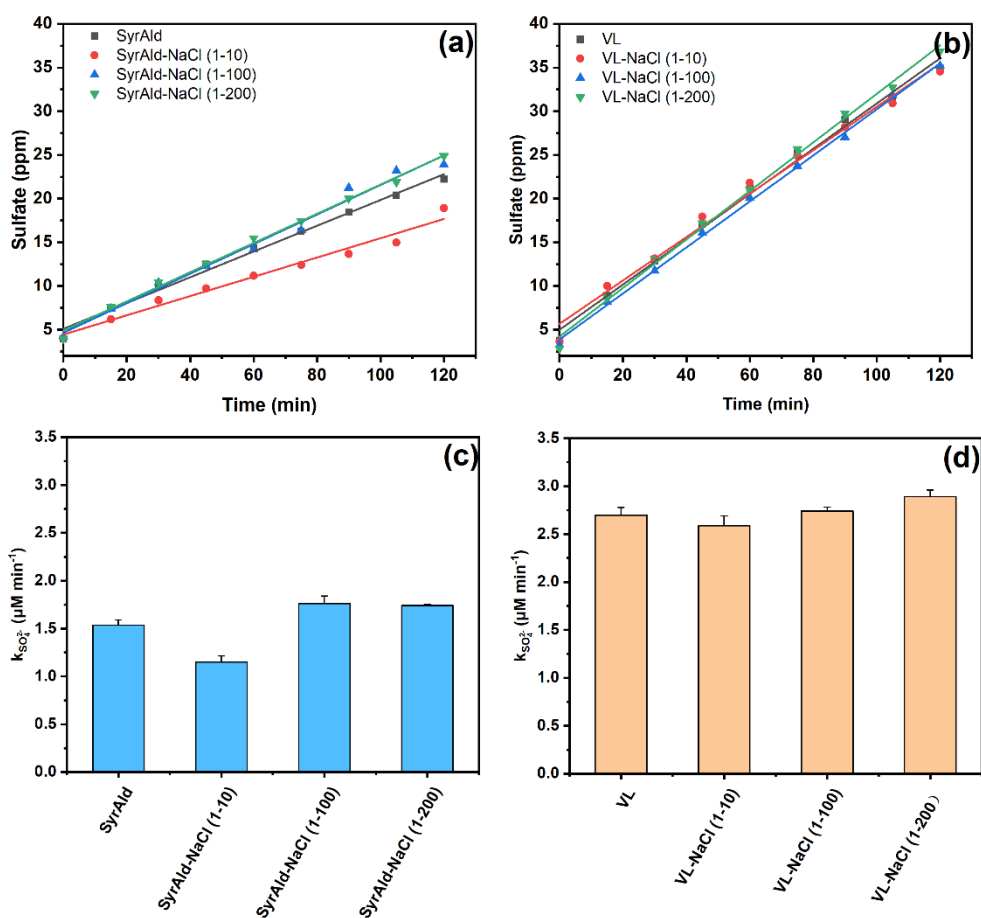
Figure S11. (a) (b) Sulfate formation and (c) (d) sulfate formation rates by different combinations of PS and chloride: (a)(c) SyrAld-NaCl; (b)(d) VL-NaCl. 1-10, 1-100 and 1-200 represent the mass ratios of different species. Among them, the concentrations of SyrAld and VL were 1 ppm, while the NaCl concentrations were varied, 10, 100 and 200 represent 10 ppm. 100 ppm and 200 ppm, respectively.
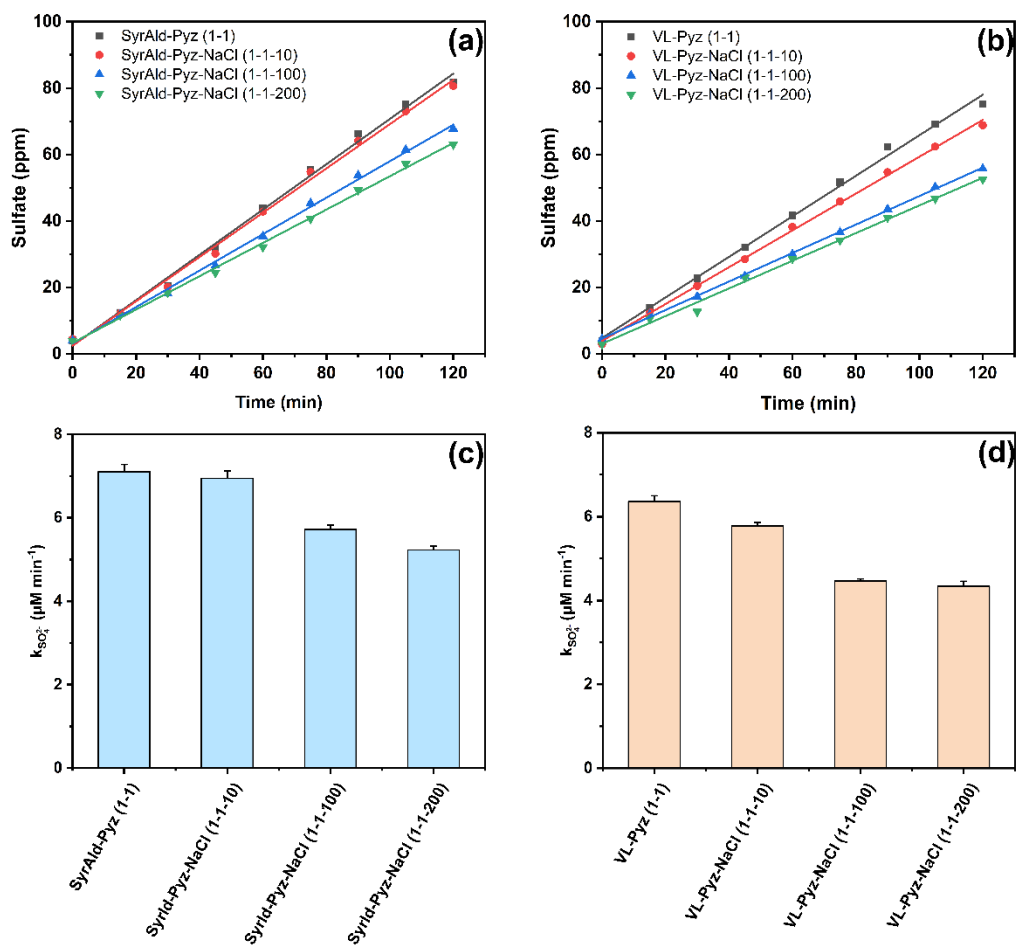
Figure S12. (a) (b) Sulfate formation and (c) (d) sulfate formation rates by different combinations of PS, CHN species and chloride: (a)(c) SyrAld-Pyz-(NaCl); (b)(d) VL-Pyz-(NaCl). 1-1-10, 1-1-100 and 1-1-200 represent the mass ratios of different species. Among them, the concentrations of SyrAld, VL and Pyz were 1 ppm, while the NaCl concentrations were varied, 10, 100 and 200 represent 10 ppm. 100 ppm and 200 ppm, respectively.
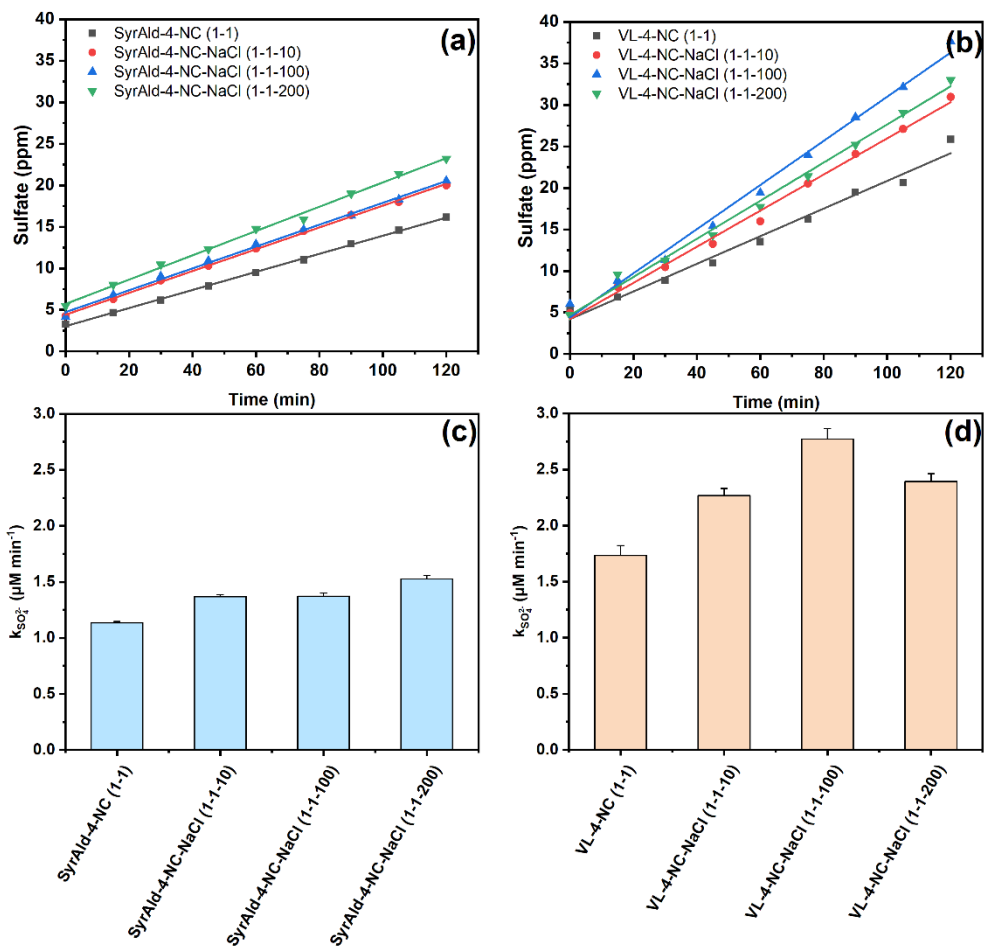
Figure S13. (a) (b) Sulfate formation and (c) (d) sulfate formation rates by different combinations of PS, CHON species and chloride: (a)(c) SyrAld-4-NC-(NaCl); (b)(d) VL-4-NC-(NaCl). 1-1-10, 1-1-100 and 1-1-200 represent the mass ratios of different species. Among them, the concentrations of SyrAld, VL and 4-NC were 1 ppm, while the NaCl concentrations were varied, 10, 100 and 200 represent 10 ppm. 100 ppm and 200 ppm, respectively.

REFERENCES

Koch, B. P. and Dittmar, T.: From mass to structure: An aromaticity index for high-resolution mass data of natural organic matter, Rapid communications in mass spectrometry, 20, 926-932, 2006.

Song, K., Gong, Y., Guo, S., Lv, D., Wang, H., Wan, Z., Yu, Y., Tang, R., Li, T., and Tan, R.: Investigation of partition coefficients and fingerprints of atmospheric gas-and particle-phase intermediate volatility and semi-volatile organic compounds using pixel-based approaches, Journal of Chromatography A, 1665, 462808, 2022a.

Song, K., Guo, S., Gong, Y., Lv, D., Zhang, Y., Wan, Z., Li, T., Zhu, W., Wang, H., and Yu, Y.: Impact of cooking style and oil on semi-volatile and intermediate volatility organic compound emissions from Chinese domestic cooking, Atmospheric Chemistry and Physics, 22, 9827-9841, 2022b.

Zhang, Y., Wang, K., Tong, H., Huang, R.-J., and Hoffmann, T.: The maximum carbonyl ratio (MCR) as a new index for the structural classification of secondary organic aerosol components, Rapid Communications in Mass Spectrometry, 35, e9113, https://doi.org/10.1002/rcm.9113, 2021.

Zherebker, A., Rukhovich, G. D., Sarycheva, A., Lechtenfeld, O. J., and Nikolaev, E. N.: Aromaticity Index with Improved Estimation of Carboxyl Group Contribution for Biogeochemical Studies, Environmental Science & Technology, 56, 2729-2737, 10.1021/acs.est.1c04575, 2022.